Charge-Localized *p*-Phenylenedihydrazine Radical Cations: ESR and Optical Studies of Intramolecular Electron Transfer Rates

**Stephen F. Nelsen,* Rustem F. Ismagilov, and Douglas R. Powell**

*Contribution from the Department of Chemistry, University of Wisconsin,
1101 University Avenue, Madison, Wisconsin 53706-1396*

Received June 19, 1997[⊗]

Abstract: 1,4-Bis(2-*tert*-butyl-2,3-diazabicyclo[2.2.2]oct-3-yl)benzene-1,4-diyl (**2**) its 2,5-dimethyl and 2,3,5,6-tetramethyl derivatives (**3** and **4**), their radical cations, and bis-radical dications are studied. Crystal structures including those of $2^+BPh_4^-$, $3^{2+}(BPh_4^-)_2$, $4^+BPh_4^-$, and $4^{2+}(BPh_4^-)_2$ establish that ring methylation causes more N-lone pair, aryl π twist without changing the N_{Ar},N_{Ar} distance significantly and that both 2^+ and 4^+ have the charge localized in one hydrazine unit. NMR measurements show that 3^+ has about 6% of its spin at the four aryl CH and CMe carbons, while 4^+ has about 1.5% of its spin at the four CMe carbons. The average distance between the unpaired electrons of 3^{2+} and 4^{2+} was obtained from the dipolar splittings of their thermally excited triplet states and, as expected, is significantly smaller for 3^{2+} (5.25 Å) than for 4^{2+} (5.63 Å). Rate constants for electron transfer between the hydrazine units of 3^+ and 4^+ in CH_2Cl_2 and CH_3CN were determined by dynamic ESR. The intervalence radical cations show charge transfer bands corresponding to vertical electron transfer between the ground state and the highly vibrationally excited electron-shifted state, allowing calculation of the parameters controlling electron transfer. Electron transfer parameters obtained from the CT bands using adiabatic energy surfaces which approximate the CT band shapes observed produce rate constants within experimental error of those extrapolated to room temperature from the ESR data for both 3^+ and 4^+ in both solvents, without using tunneling corrections. The effects of mixing of the electronic wave functions of the reduced and oxidized hydrazine units of 2^+ on d_{NN}, the C(*t*-Bu)N,NA(Ar) twist angle, and the aryl nitrogen lone pair, aryl π twist angle which are observed by X-ray are close to those predicted from the position of the minima on the ET coordinate X of the adiabatic energy surface calculated from the CT band.

Introduction

We previously reported that in contrast to the radical cation of tetramethyl-*p*-phenylenediamine (1^+) in which the charge and spin are delocalized over the eight atom π system, its bis-hydrazine analogue, 2^+, has charge and spin instantaneously
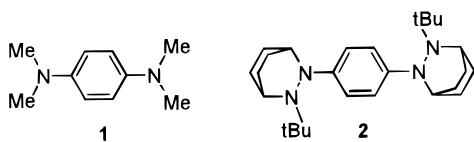
localized on one of the hydrazine units, although the electron transfer (ET) which interconverts the hydrazine units is fast on the ESR time scale at −78 °C.[1] This paper provides a more complete account of this work, as well as ESR and optical studies on the ring-methylated analogues 3^+ and 4^+, which
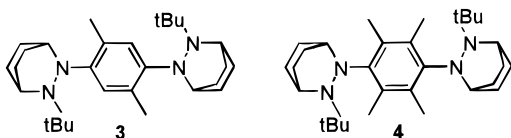

undergo slower ET and allow comparison of the rate constant for intermolecular ET, k_{et}, with theoretical predictions arising from analysis of the charge transfer (CT) absorption bands for these π-linked systems. A new analysis of CT bands using

adiabatic theory based upon quartic-augmented diabatic energy curves instead of the Marcus/Hush parabolas allows calculation of band shape for the CT bands to be used in extracting the ET parameters, which brings the calculated ET rate constants into excellent agreement with the experimental ones.

Results: Preparation and Oxidation Thermodynamics

Compounds **2**−**4** were made by addition of aryldilithiums prepared from the aryl diiodides[2,3] to 2-*tert*-butyl-2,3-diazabicyclo-[2.2.2]oct-2-ene iodide, and the monohydrazine **5** was prepared
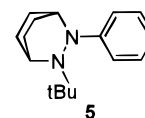

similarly. The bis-hydrazines are too air sensitive for convenient chromatography, and crystallization from toluene/acetonitrile is a convenient way to purify them. The hydrazine units of **2** are twisted out of the aromatic ring plane and can exist in *meso* and *d,l* nitrogen inversion diastereomers, each of which can have *syn* or *anti* N−Ar rotation conformations, as shown in Scheme 1. Each of the four species in Scheme 1 has two different $C_{Ar}H$ carbons, all of which are resolved in a δ 1.27 range of the ^{13}C NMR spectrum at −32 °C in CD_2Cl_2 and have equal intensities.[1] The presence of these diastereomers in solution is not energetically significant in the sense that the free energy is not affected

[⊗] Abstract published in *Advance ACS Abstracts,* October 1, 1997.
(1) Nelsen, S. F.; Ismagilov, R. F.; Powell, D. R. *J. Am. Chem. Soc.* **1996**, *118*, 6313.

(2) Suzuki, H.; Nakamura, K.; Goto, R. *Bull. Chem. Soc. Jpn.* **1966**, *39*, 128.
(3) Platt, K. L.; Setiabudi, F. *J. Chem. Soc., Perkin Trans. 1* **1992**, 2005.

Scheme 1. Diastereomers of **2**
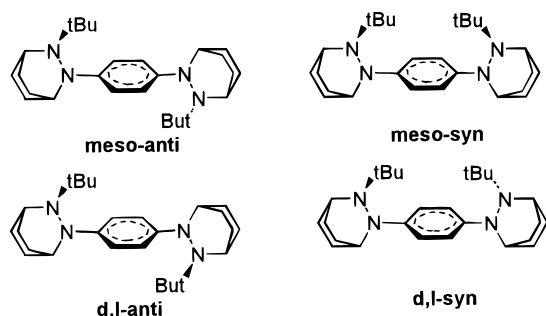
by the double nitrogen inversion or *syn,anti* rotation forms of the hydrazine units relative to each other. The double nitrogen inversion which interconverts the *meso* and *d,l* diastereomers remains slow on the NMR time scale even at high temperatures, but *syn,anti* interconversion becomes rapid at 80 °C in benzene, where the *C*N quaternary carbons for the *meso* and *d,l* diastereomers are sharp ($\Delta\delta = 0.09$), but the $C_{Ar}H$ signals have merged and are only slightly broadened. The ^{1}H NMR shows complex fine structure for the aromatic signals at −78 °C in CD_2Cl_2, but the fine structure disappears as the temperature is raised, and by 25 °C, only two broad signals for $C_{Ar}H$ *syn* and *anti* to the *tert*-butyl group appear. In C_6D_6 at 25 °C and 500 MHz, the upfield $C_{Ar}H$ signal is split into two broad singlets, with a separation of 30 Hz, centered 494 Hz from the downfield $C_{Ar}H$ signal. The coalescence temperature for these signals is 77 ± 2°, corresponding to a $C_{Ar}-N$ rotational barrier of 15.23 ± 0.04 kcal/mol. The $C_{Ar}-N$ rotational barrier is even higher for the tetramethyl compound **4**, which at room temperature shows two sets of four equal intensity methyl signals at δ 3.08− 3.00 and 2.53−2.49 by ^{1}H NMR and 4 $C_{Ar}N$, 8 $C_{Ar}H$, and 8 $C_{Ar}CH_3$ signals by ^{13}C NMR. The dimethyl compound **3** shows only pairs of $C_{Ar}N$, $C_{Ar}H$, and $C_{Ar}CH_3$ signals, indicating that only one $C_{Ar}-N$ rotamer is detectably occupied for each N inversion diastereomer. This is presumably the less hindered one, having the N-*t*-Bu group *syn* to the hydrogen-substituted ortho position, which was the rotamer observed in a poor crystal structure of **3** (see below).

The cyclic voltammograms for **2−4** show two chemically and electrochemically reversible waves (see Table 1). Including the 0.018 V statistical correction for the two hydrazine units of **2**, it loses an electron in acetonitrile (AN) 0.15 V (3.6 kcal/mol) more easily than its monohydrazine analogue **5**, presumably because of stabilization of the oxidized hydrazine unit by electron release from the reduced unit to the aromatic ring. Stable radical cation solutions are critical for accurate optical and ESR studies, but it was found that the lifetime of solutions of **2**$^+$ prepared by various oxidation methods were variable. The green color of **2**$^+$ typically persists for tens of minutes in solution with no detectable change in the optical spectrum, but once **2**$^+$ starts decomposing, the rate of its decomposition increases. The dication **2**$^{2+}$ decomposes with a half-life of tens of seconds, we believe releasing protons because of *tert*-butyl cation loss, and acid catalyzes the decomposition of **2**$^+$. We are still investigating the decomposition pathways for **2**$^+$. Solutions of **3**$^+$, **4**$^+$, and **5**$^+$ are stable for many days, and both **3**$^{2+}$ and **4**$^{2+}$ proved isolable. The effect of ring methylation on the thermodynamics of electron loss from **2−4** was examined in acetonitrile and methylene chloride (MC) (see Table 1). The first pair of ring methyls (**2 → 3**) makes first electron removal more facile by 1.4 kcal/mol in AN and 0.7 kcal/mol in MC, while the second pair (**3 → 4**) decreases $E^{\circ\prime}_1$ an additional 4.6 (AN) to 5.1 (MC) kcal/mol. Both "inductive" (Me stabilizes

positive charge better than H) and inhibition of resonance (Me causes greater twist about the N−Ar bond) effects are involved, but the significantly greater contribution of the second pair of methyls to lowering $E^{\circ\prime}$ indicates that resonance is the more important effect. The second pair of methyls must be introduced *syn* to the bulkier N-*t*-Bu side of the bicyclooctyl ring. Steric inhibition of resonance from greater twisting caused by the methyl groups presumably lowers $E^{\circ\prime}_1$ due to greater destabilization of the neutral form relative to the more twisted oxidized form present in the radical cation. The methylation effect on second electron removal is close to that on the first, and $\Delta E^{\circ\prime} = (E^{\circ\prime}_2 - E^{\circ\prime}_1)$ is 6.5 ± 0.5 kcal/mol for **2−4** in AN, but is significantly larger in MC, 8.5 ± 0.5 kcal/mol. $E^{\circ\prime}_1$ is 0.05− 0.08 V larger in MC than in AN for **2−4**, compared to 0.10 V for the monomeric hydrazine **5** and 0.07 and 0.10 for decamethylferrocene and ferrocene (see Table 1). The effect of changing solvent upon $E^{\circ\prime}_2$ is somewhat larger, a 0.11−0.17 V increase in going from AN to MC for **2−4**. This suggests to us that the oxidized hydrazine units may be specifically stabilized by the more donating solvent, AN. Effects of other solvents on the thermodynamics of electron removal will be discussed elsewhere.

Results and Discussion: Crystal Structures

The amount of twist at the $C_{Ar}-N$ bonds and the distance between the hydrazine units are important for determining the ET rate, and we have characterized several of these compounds by X-ray crystallography. We especially wanted to obtain crystals of the radical cations. As has often been a problem for coordination complex intervalence compounds,[4] despite ET disproportionation being endothermic in solution, the disproportionation products usually crystallize. Crystallization of BF_4^- and PF_6^- salts of **2**$^+$ led only to **2**^{0} and **2**$^{2+}$ decomposition products crystallizing instead of the desired **2**$^+$. By having **2**^{0} present (which protects **2**$^+$ from decomposition), selecting the counterion Ph_4B^- (which is comparable in size to **2** so that packing does not greatly favor $2^{2+}(X^-)_2$ over 2^+X^-), and crystallizing by diffusion of the more polar water into the less polar AN (favoring crystallization of the less polar **2**$^+$ over the more polar **2**$^{2+}$, which crystallizes when the more usual reversed polarity crystallization is carried out), X-ray-quality green crystals of $2^+BPh_4^-$ could be picked from the colorless **2**^{0} crystals initially present. The same procedure also allowed isolation of $4^+(BPh_4^-)$ as the intervalence salt, but it unfortunately has failed so far for $3^+BPh_4^-$. Although dark crystals which dissolve to give **3**$^+$ solutions are obtained, picking well-formed crystals from the mass has produced crystal structures of 3^{2+} $(BPh_4^-)_2 \cdot (CH_3CN)_2$ on two separate tries.

We have been unable to obtain a crystal structure of the low-melting **5**^{0} and not succeeded in solving the crystal structure of **4**^{0}, apparently because of severe disorder problems. A solution was obtained for the structure of **3**^{0}, but the crystal was twinned and disordered and produced σ values of 0.006−0.008 Å for the bond lengths. The structural parameters are not reliable and are not reported in detail, but the two crystallographically independent **3**^{0} units in this poor crystal structure are in the expected $C_{Ar}-N$ rotamer, with N-*t*-Bu *syn* to an ortho CH group.

As shown in Table 2, the geometry of one hydrazine unit of **2**$^+$ closely resembles that of **2**^{0} and the other that of **5**$^+$, conclusively demonstrating that charge localization occurs and is associated with the green color. The presence of the counterion reduces disorder at an oxidized hydrazine unit because the oxidized hydrazine unit of $4^+BPh_4^-$ is not disordered, although the neutral unit was found in three orientations

(4) Creutz, C. *Prog. Inorg. Chem.* **1983**, *30*, 1.

Table 1. Comparison of Cyclic Voltammetry Data for **2**−**5** in Acetonitrile (AN) and Methylene Chloride (MC)[a]

	$E°'_1(AN)^b$	$E°'_2(AN)^b$	$\Delta E°'(AN)$	$E°'_1(MC)^b$	$E°'_2(MC)^b$	$\Delta E°'(MC)$
2	+0.09 (0.06)[c]	+0.39 (0.07)	0.30	+0.14 (0.12)[c]	+0.51 (0.10)	0.37
3	+0.03 (0.06)[c]	+0.33 (0.07)	0.30	+0.11 (0.08)[c]	+0.50 (0.07)	0.39
4	−0.17 (0.07)[d]	+0.09 (0.07)	0.26	−0.14 (0.07)[d]	+0.24 (0.07)	0.35
5	+0.26 (0.07)[d]			+0.36 (0.09)[c]		

[a] Containing 0.1 M tetrabutylammonium chloride as supporting electrolyte, potentials reported in V vs a saturated calomel electrode. [b] Calculated as $(E_p^{ox} + E_p^{red})/2$. The number shown in parentheses is $(E_p^{ox} - E_p^{red})$. [c] Decamethylferrocene used as internal standard, $E°(AN) = -0.11$, $E°(MC) = -0.04$ V vs SCE. [d] Ferrocene used as internal standard, $E°(AN) = +0.40$, $E°(MC) = +0.50$ V vs SCE.

Table 2. Comparison of Geometries about the Nitrogens for *p*-Phenylenedihydrazines[a]

	unit	$d(NN)$	$d(NC_{Ar})$	$\alpha_{av}(NBu)$	$\alpha_{av}(NAr)$	ψ_{CNNC}	$\phi_{lp,\pi}$
2^0	neu.	1.461(2)	1.440(2)	113.1(1)	112.0(1)	−105.8(1)	−37.5(2)
2$^+$BPh$_4^-$	neu.	1.454(3)	1.426(3)	113.6(2)	112.7(2)	−107.3(3)	−32.6(3)
	cat.	1.359(3)	1.436(3)	118.7(2)	116.2(2)	+67.3(3)	+47.6(3)
5$^+$NO$_3^-$	cat.	1.355(2)	1.440(2)	119.1(1)	117.0(1)	−53.6(2)	−59.2(2)
5$^+$B(C$_2$H$_4$)$^-$	cat.	1.351(2)	1.443(3)	119.3(2)	117.2(2)	+57.5(3)	+53.1(3)
3^{2+}(BPh$_4^-$)$_2^b$	cat.	1.354(2)	1.432(3)	119.1(2)	117.5(2)	+54.8(3)	+57.4(2)
4$^+$BPh$_4^-$	neu. A	1.456(6)	1.459(5)	112.2(4)	114.3(4)	−91.4(5)	−53.2(8)
	neu. B	1.440(9)	1.459(4)	113.1(6)	113.2(7)	−99.3(9)	−45.9(13)
	neu. C	1.442(8)	1.460(4)	114.0(5)	113.5(6)	+91.0(7)	+52.3(14)
	cat.	1.346(2)	1.455(3)	118.6(2)	119.0(2)	−44.8(3)	−66.2(3)
4^{2+}(BPh$_4^-$)$_2$	cat.	1.356(3)	1.443(3)	118.5(2)	118.5(3)	−48.0(4)	−63.6(4)

[a] The authors have deposited atomic coordinates for these structures with the Cambridge Crystallographic Data Centre. The coordinates may be obtained, upon request, from the Director, Cambridge Crystallographic Data Centre, 12 Union Road, Cambridge CB2 1EZ, U.K. [b] Two CH$_3$CN are also present in the unit cell. See footnote a of Table 3.

Table 3. Intramolecular Nonbonded N,N Distances for **2**^{0}, **2**$^+$, **4**$^+$, and **4**$^{2+}$

	$d(N_{Ar},N_{Ar})$	$d(N_{tBu},N_{tBu})$
2^0	5.702	7.423
2$^+$BF$_4^-$	5.657	6.989
3^{2+}(BPh$_4^-$)$_2^a$	5.616	7.362
4$^+$BPh$_4^-$,A	5.681	7.535
4$^+$BPh$_4^-$,B	5.713	7.557
4$^+$BPh$_4^-$,C	5.624	7.570
4^{2+}(BPh$_4^-$)$_2$	5.673	7.535

[a] Two CH$_3$CN are also present in the unit cell. A separate determination on a different crystal gave 5.641 and 7.399 Å, respectively, and all of the parameters from Table 1 the same except $d(NN)$ = 1.365(2) and $d(NC_{Ar})$ = 1.439(2).

relative to the oxidized unit, A:B:C in relative amounts 0.45: 0.23:0.30. The bond lengths and average of the bond angles at nitrogen, α_{av}, for the reduced and oxidized units of both **2**$^+$ and **4**$^+$ closely resemble those for the neutral and cationic models. The twist angles are "softer" and show greater variation between similarly substituted examples. The exocyclic $C_{tBu}N,NC_{Ar}$ twist angle ψ_{CNNC} has an electronically preferred value of 0° in the cationic units, but severe steric interactions prevent it from approaching this value very closely, although ψ_{CNNC} is 40° smaller for the oxidized than the reduced unit of **2**$^+$ and 46−55° smaller for **4**$^+$. Conjugation of the N$_{Ar}$ lone pair with the aromatic ring is poorer for oxidized than for reduced hydrazines, and the N$_{Ar}$ lone pair, C$_{Ar}$ p orbital twist angle $\phi_{lp,\pi}$ at the oxidized hydrazine unit is 15° larger for **2**$^+$ and 13−20° larger for **4**$^+$. The ring methyl substitution in going from **2**$^+$ to **4**$^+$ increases $\phi_{lp,\pi}$ by about 18° at both the reduced and oxidized hydrazine units, and $\phi_{lp,\pi}$ at oxidized hydrazine units increases 6.2° in going from the dimethyl substituted **3**$^{2+}$ to the tetramethyl substituted **4**$^{2+}$. The distance between the charge-bearing hydrazine units is significant for ET considerations, and the N,N distances obtained from the crystal structures are summarized in Table 3. As anticipated, the distance between the N-Ar nitrogens depends little upon either ring methyl substitution or oxidation state, averaging to 5.67 Å, with values near the extremes, 5.71 and 5.62, occurring for different diastereomers of **4**$^+$.

Results and Discussion: Spin Density Distribution in the Radical Cations

It is necessary to know the ESR splitting constants for accurate simulation of dynamically broadened ESR spectra. There are so many hydrogen splittings that the only lines resolved in the ESR spectra of these compounds are the large nitrogen splittings, and the difference between the two types of N present was not resolved.[1] Despite considerable effort (by Franz Neugebauer, MPI Heidelberg), **2**$^+$−**4**$^+$ have not yet shown any ENDOR signals. The ^{1}H NMR spectra of these compounds allow determination of $a(H)$ values because paramagnetic shifts $\Delta\delta_p$ for a radical at 300 K are δ 73.76/G of ESR splitting $a(H)$, although because line width increases roughly as $(\Delta\delta_p)^2$, only the signals for rather small $a(H)$ protons can usually be observed.[5,6] Addition of di-*tert*-butyl nitroxide as a spin relaxant to sharpen the lines allows detection of signals for protons having $a(H)$ up to ca. 1.5 G, and **2**$^+$−**4**$^+$ have small enough reduction potentials that it could be employed. Because double nitrogen inversion is slow on the NMR time scale, there is no symmetry in the bicyclooctyl rings, and because ET between the two hydrazine units is fast on the NMR time scale, these protons are averaging between the values for the oxidized and reduced rings, the latter being zero. Table 4 summarizes the splitting constants derived from NMR experiments. This experiment was least satisfactory for **2**$^+$, which is in the intermediate N,C$_{Ar}$ rotation region for its proton NMR and for which we could only observe a single broad line for the *exo* bicyclic ring protons and no signal for the aromatic hydrogens. In contrast, signals for the *exo* hydrogen splittings, which are sensitive to lone pair alignment,[6b] were resolved for both **3**$^+$ and **4**$^+$. The *endo* bicyclic ring proton splittings, which are negative, small, and not very sensitive to lone pair alignment[6b] were not completely resolved for **3**$^+$, and only a single broad signal was observed for **4**$^+$.

(5) Kreilick, R. W. *NMR of Paramagnetic Molecules*; La Mar, G. N., Horrocks, W. DeW., Jr; Holm, R. H., Eds.; Academic Press: New York, 1973; Chapter 15, p 595.
(6) (a) Petillo, P. A.; De Felipppis, J.; Nelsen, S. F. *J. Org. Chem.* **1991**, *56*, 6496. (b) Nelsen, S. F.; Petillo, P. A.; De Felipppis, J.; Wang, Y.; Chen, L.-J.; Yunta, M. J. R.; Neugebauer, F. *J. Am. Chem. Soc.* **1993**, *115*, 5608.

Table 4. NMR-Derived ESR a_H Values (G) for 2^+-4^+

	2^+	3^+	4^+
$a(H_{exo})$	(unres.)	1.54,1.18	1.23,1.09
		0.93,0.66	0.81,0.71
$a(H_{exo})$[av]	[1.03]	[1.08]	[0.96]
$a(H_{endo})$[av]	[−0.25]	[−0.3]^a	[−0.24]
$a(t\text{-Bu})$	+0.108	+0.107	+0.097
$a(H_{br})$	(unobs.)	−0.07?	(unobs)
$a(MeAr)$	—	0.266,0.189	0.171,0.157
$a(MeAr)$[av]	—	[+0.228]	[+0.164]
$a(HAr)$	(unobs.)	−0.656,−0.607	—
$a(HAr)$[av]		[−0.631]	

^{a} Signals corresponding to splittings of −0.24, −0.329, and −0.370 were observed and presumably correspond to *endo* splittings.

The aromatic methyl and $C_{Ar}H$ protons were resolved for both 3^+ and 4^+. Although assignment of ortho and meta splittings in the frozen spectrum cannot be made because only equilibrating species are observed, there is clearly more spin density in the aryl ring of 3^+ than of 4^+. Using Q_H at 26.64 G (that for $C_6H_6^+$) and Q_{Me} at 43.6 G (that for $C_6Me_6^+$ and $C_2Me_4^+$)[7] with $a(H) = Q_x\rho_{CX}^\pi$, the 3^+ splittings give average ρ_{CH}^π of 0.0237 and ρ_{CMe}^π of 0.0066, corresponding to 6.0% of the electron spin density at the four labeled positions, while the average ρ_{CMe}^π for 4^+ is 0.0038, corresponding to 1.5% of the electron spin density at the four methylated positions.

Results: Dynamic ESR Measurements of k_{et}

The rate region for which the ESR spectrum is most sensitive to exchange is that near $k_{et} \sim 10^8$ s^{-1} for these [$a(2N) \sim 13$ G]$\rightleftharpoons$[$a(2N) \sim 0$ G] systems, where the intermediate lines of the $\sim$6.5 G separation nine line fast-ET spectrum change in size most rapidly during the change to the $\sim$13 G separation five-line slow-ET spectrum.[8] 2^+ has a k_{et} value too large to see significant distortion of the fast-ET spectrum near the melting point of both acetonitrile (AN, mp 229 K) and methylene chloride (MC, mp 176 K). The solvent reorganization energy is enough lower in MC than AN that being able to cool an additional 50 °C does not lead to significantly slower ET. Acetone (mp 178 K) causes a solvent reorganization energy only slightly lower than AN, and by adding enough AN to depress the melting point, we were able to show that 2^+ is localized in solution by obtaining a very broadened five-line slow-ET spectrum at 168 K in 12:1 acetone:AN.[1] ET is enough slower for 4^+ that the exchange rate sensitive region comes near 200 K in MC and 250 K in AN. 4^+ ESR spectra in these regions are rather well fit (see Figure 1) using dynamic exchange between the units of a localized species with $a(2N) = 13.1$, $a(4H) = 1.96$, $a(4H) = 0.48$ G and a line width of 1.7−1.8 G; the k_{et} values obtained are summarized in Table 5. The 3^+ spectra are not fit quite as well using simulation parameters of $a(2N) = 13.1$, $a(4H) = 1.96$, $a(4H) = 0.48$ G and a line width of 1.7−1.8 G, probably because of larger aromatic ring splittings (which we do not know) for the localized species, but as seen in Table 5, the estimated k_{et} values for 3^+ and 4^+ are probably within experimental error of being the same. Only 19−30° temperature ranges are available, making the activation parameters derived from the measured rate constants rather inaccurate. The temperature ranges for which the spectra are sensitive to changing temperature so k_{et} can be estimated do not overlap in the two solvents because k_{et} is higher in MC than in AN (at 225 K, between the temperature ranges studied, by a factor of
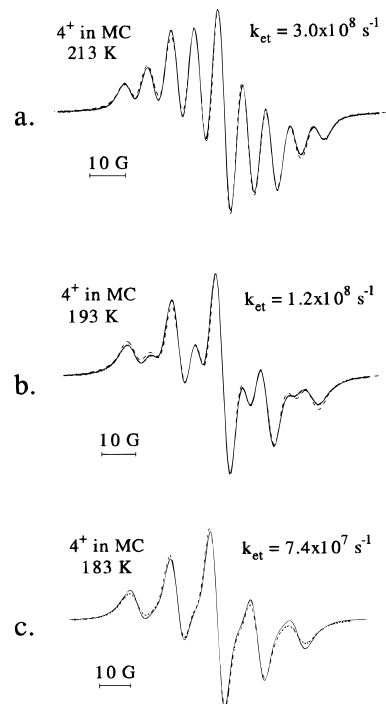
(7) Gerson, F.; Gescheidt, G.; Nelsen, S. F.; Paquette, L. A.; Teasley, M. F.; Waykole, L. *J. Am. Chem. Soc.* **1989**, *111*, 5518.

(8) Nelsen, S. F.; Wolff, J. J.; Chang, H.; Powell, D, R. *J. Am. Chem. Soc.* **1991**, *113*, 7882.


Figure 1. ESR spectra for 4^+ in methylene chloride compared with simulations (dashed lines) for a hydrazine unit with $a(2N) = 13.1$, $a(4H) = 1.96$, and $a(4H) = 0.48$ G, dynamically exchanging with one having zero splittings for (a) $k_{et} = 3.0 \times 10^8$ s^{-1}, line width = 1.7 G, at 213 K; (b) $k_{et} = 1.20 \times 10^8$ s^{-1}, line width = 1.7 G, at 193 K; and (c) $k_{et} = 7.40 \times 10^7$ s^{-1}, line width = 1.8 G, at 183 K.

Table 5. Summary of Dynamic ESR Results

	3^+	3^+	4^+	4^+
solvent	AN	MC	AN	MC
k_{et}, 10^8 s^{-1} $(T,$ K)		2.75 (212)	2.64 (265)	2.99 (213)
		2.03 (202)	2.13 (260)	2.38 (208)
	1.99 (255)	1.65 (198)	1.76 (255)	1.94 (203)
	1.55 (245.6)	1.34 (192)	1.44 (250)	1.57 (198)
	1.36 (241)	1.06 (187)	1.14 (245)	1.20 (193)
	1.18 (236)		0.77 (236)	0.74 (183)
Extrapolated Values				
$\Delta H^\ddagger$, kcal/mol^a	2.81(4)	2.65(25)	4.76(24)	3.21(11)
$\Delta S^\ddagger$, eu^a	−9.2(2)	−6.7(13)	−1.8(10)	−4.1(5)
k_{et}, 10^8 s^{-1} (200 K)	0.34	1.80	0.105	1.72
k_{et}, 10^8 s^{-1} (260 K)	2.30	11.0	2.18	14.1
k_{et}, 10^{-8} s^{-1} (298 K)	5.2	24	8.1	36

^{a} Numbers in parentheses refer to statistical error only in the last place quoted; real errors are doubtlessly larger.

about 5 for 3^+ and 10 for 4^+). We note that 3^+ is predicted to have higher k_{et} than 4^+ at 200 K and the reverse to be true at room temperature in both solvents.

Results: Dipolar Splittings of Triplets 4^{2+} and 3^{2+}

Although the bis-radical cation 4^{2+} is isolable as the (BPh$_4^-$)$_2$ salt, 4^{2+} is very slowly reduced in AN solution by this counterion to generate the characteristic green color of cation 4^+. Solutions of 4^{2+}(SbF$_6^-$)$_2$, prepared by oxidation of 4^0 with 2 equiv of AgSbF$_6$, are more stable. The solution ESR spectrum of 4^{2+} at room temperature resembles that of 4^+ but is broadened, probably from incomplete averaging of the dipolar splitting. The spectrum in acetonitrile at 77 K shows a superposition of a triplet and a much larger, narrower central g = 2 line, and the relative intensity of these two species varied with sample. Only the central line was observed for crystalline 4^{2+} salts, making it likely that the triplet spectrum arose from
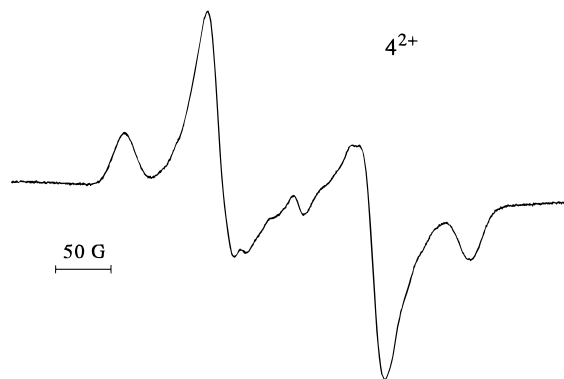
Figure 2. ESR spectrum of $4^{2+}(SbF_6^-)_2$ at 77 K in a 1:1:1 AN: butyronitrile:MC glass.

regions that had glassed, and the central line from polycrystalline material. The largest triplet lines were about the same height as the central one in MC, and a rapidly cooled 1:1:1 AN: butyronitrile:MC mixture gave a spectrum with the central line almost absent (Figure 2). The separation of the outer lines, 311 G, is twice the zero-field dipolar splitting parameter $D' = 155$ G. From the point dipole approximation,[9] the distance d_{esr} between two localized radicals is 30.3 $D'^{-1/3}$, corresponding to $d_{esr} = 5.63$ Å, which almost equal to the X-ray crystallographic $d(N_{Ar},N_{Ar}')$ for $4^{2+}(BPh_4^-)_2$ of 5.673 Å (0.8% shorter). Although d_{esr} for a dication is completely experimentally independent from the average distance d between the charge-bearing centers in the radical cation which is necessary for application of ET theory (see below), the assumptions about average distance seem to be very similar. The triplet spectrum of 4^{2+} therefore provides powerful support for using the X-ray $d(N_{Ar},N_{Ar}')$ as d for 4^+ instead of a larger number, such as $d(N_{tBu},N_{tBu}')$ or the distance between the midpoints of the NN bonds.

The triplet ESR spectrum of 3^{2+} in a 1:1 AN:PrCN glass has a lower intensity than that of 4^{2+}, and a spectrum as free of the central line was not obtained. The triplet spectrum intensity improves up to about 160 K, but the glass melts and the triplet spectrum disappears at higher temperatures. The D' value of 192 G corresponds to a d_{esr} value of 5.25 Å. This is 6.5% smaller than the X-ray crystallographic $d(N_{Ar},N_{Ar}')$ of 5.616 Å. Although the $d(N_{Ar},N_{Ar}')$ value for 3^{2+} is only 0.057 Å smaller than that for 4^{2+}, the d_{esr} value for 3^{2+} is 0.38 Å smaller than that for 4^{2+}. This is consistent with the slightly smaller twist for 3^{2+} than for 4^{2+} found by crystallography ($\phi_{lp,\pi}$ is 6.2° smaller) leading to more spin delocalization into the aromatic ring, as indicated by the NMR measurements of spin density in the radical cations. These studies on the dications indicate that the electron transfer distance d required for extraction of V from the optical data of the radical cations should be smaller for 3^+ than for 4^+, and in the discussion below, we shall use the d_{esr} value for d of the radical cation.

We were unable to observe a triplet ESR spectrum for 2^{2+} in glasses. The singlet, triplet separation for this species is presumably larger for 2^{2+} than for the more twisted 3^{2+} and 4^{2+}, resulting in significantly smaller amount of the triplet being present at the low temperatures necessary to maintain the glasses used. The samples of 2^{2+} readily decompose upon warming to room temperature, as shown by their optical spectra. In work to be published later, d_{esr} for the 4,4′-biphenyl-bridged analogue of 2^{2+} has been shown to be only about 0.81 times as large as

the crystallographic $d(N_{Ar},N_{Ar}')$, which is consistent with the substantially smaller twist for systems lacking aromatic methyl groups. Using this factor corresponds to an effective d of about 4.6 Å for 2^+, which we use below in estimating V for 2^+.

Results and Discussion: Evaluation of V from the CT Bands for 2^+–4^+

2^+–4^+ show broad optical bands reaching maxima between ca. 700 and 900 nm, which we assign as Hush-type CT bands, corresponding to vertical excitation from the charge-localized ground state to highly excited vibrational levels of the electron-transferred state. They are organic analogues of symmetrical transition metal intervalence complexes,[4] to which Marcus/Hush theory[10] and its more recent extensions should apply for extraction of the fundamental ET parameters from which k_{et} ought to be calculable. These parameters are the matrix element coupling the charge-bearing units (through the linking unit in our intervalence compounds), V; the total vertical reorganization energy, λ, which consists of the internal vibrational reorganization energy, λ_v, and the solvent reorganization energy, λ_s ($\lambda = \lambda_v + \lambda_s$); and the averaged energy of the vibrations activated in transferring the electron, $h\nu_v$.[10]

Hush pioneered theoretical treatment of intervalence complex absorption bands.[11] The expression usually employed for evaluation of V is eq 1, originally from Mulliken.[12] Although

$$V_H \ (cm^{-1}) = (0.0206/d)(E_{op}\Delta\nu_{1/2}\epsilon_{max})^{1/2} \qquad (1)$$

the original derivation assumed it to be valid only in the perturbation limit, Creutz and co-workers have shown eq 1 to be valid for Gaussian-shaped bands in the two-state model for any size V if the diabatic wave functions are orthogonal.[13] In eq 1 d (Å) is the distance an electron is transferred, E_{op} is the transition energy at the band maximum (cm^{-1}), $\Delta\nu_{1/2}$ is the band width at half height (cm^{-1}), and ϵ_{max} is the molar extinction coefficient (M^{-1} cm^{-1}) at the band maximum.

A more recent vibronic coupling theory[14] treatment by Young and co-workers[15] gives a rather different-looking expression which employs the Franck–Condon factor instead of $\Delta\nu_{1/2}$, but when compared with eq 1 for σ-linked bis-hydrazine and bis-diazenium radical cations produces results within a few percent of eq 1 except for the introduction of dependence of V on the refractive index of the solvent, which does not appear in eq 1, lowering the estimate of V. Written for the classical analysis used here, $V_L = V_H/(n_D)^{1/2}$.[16] It is not clear whether the $(n_D)^{-1/2}$ factor should be included in evaluation of V or not, and we shall examine both V_H and V_L values for estimation of rate constants.

In these expressions the CT band intensity is determined by V, which is proportional to $(\epsilon_{max})^{1/2}$. Ring methylation in the series $2^+ \rightarrow 3^+ \rightarrow 4^+$ clearly decreases V (see Figure 3), as

(9) (a) Hirota, N.; Weissman, S. I. *J. Am. Chem. Soc.* **1964**, *86*, 2538. (b) Dvolaitzky, M.; Chiarelli, R.; Rassat, A. *Angew. Chem., Int. Ed. Engl.* **1992**, *31*, 180.

(10) The standard ET theory reviews remain: (a) Marcus, R. A.; Sutin, N. *Biochim. Biophys. Acta* **1985**, *811*, 265. (b) Sutin, N. *Prog. Inorg. Chem.* **1983**, *30*, 441.

(11) (a) Hush, N. S. *Prog. Inorg. Chem.* **1967**, *8*, 391. (b) Hush, N. S. *Coord. Chem. Rev.* **1985**, *64*, 135.

(12) (a) Mulliken, R. S. *J. Am. Chem. Soc.* **1952**, *64*, 811. (b) Mulliken, R. S.; Person, W. B. *Molecular Complexes*; Wiley: New York, 1969.

(13) Creutz, C.; Newton, M. D.; Sutin, N. *J. Photochem. Photobiol. A.: Chem.* **1994**, *82*, 47.

(14) (a) Jortner, J.; Ulstrup, J. *J. Chem. Phys.* **1975**, *63*, 4358. (b) Jortner, J.; Bixon, M. *J. Chem. Phys.* **1988**, *88*, 167. (c) Cortes, J.; Heitele, H.; Jortner, J. *J. Phys. Chem.* **1994**, *98*, 2527.

(15) Gould, I. R.; Noukakis, D.; Gomez-Jahn, L.; Young, R. H.; Goodman, J. L.; Farid, S. *Chem. Phys.* **1993**, *176*, 439.

(16) (a) Nelsen, S. F.; Ramm, M. T.; Powell, D. R. *J. Am. Chem. Soc.* **1997**, *119*, 6863. (b) Nelsen, S. F.; Trieber, D. A., II; Powell, D. R. *J. Am. Chem. Soc.* **1997**, *119*, 6873.

Table 6. CT Band Data and Analysis Using Adiabatic Energy Surfaces

	2^+		3^+		4^+	
	AN	MC	AN	MC	AN	MC
Experimental Data						
λ_{max}	769	928	701	801	708	792
E_{op}, 10^3 cm^{-1}	13.0	10.8	14.3	12.5	14.1	12.6
ϵ, M^{-1} cm^{-1}	3800	5500	2100	2400	970	1080
$\Delta\nu_{1/2}$, 10^3 cm^{-1}	6.46	5.70	6.58	6.51	7.89	7.67
asymmetry[a]	0.034	0.130	0.058	0.045	(0.113)	(0.080)
Adiabatic Band Shape Analysis						
C	0.115	0.14	0.07	0.135	0.20	0.275
λ, 10^3 cm^{-1}	13.22	11.12	14.34	12.66	14.23	12.77
kcal/mol	37.8	31.8	41.10	36.15	40.75	36.50
$\lambda - E_{op}$[b]	0.6[1.9]	1.0[2.4]	0.2[1.7]	0.5[2.3]	0.3[2.7]	0.4[3.1]
d, Å	4.8	4.8	5.25	5.25	5.657	5.657
V_H [V_L][c]	2.51 [2.18]	2.60 [2.18]	1.71 [1.48]	1.71 [1.43]	1.15 [0.99]	1.16 [0.97]
kcal/mol	7.18 [6.24]	7.44 [6.24]	4.88 [4.22]	4.90 [4.10]	3.29 [2.84]	3.31 [2.77]
ΔG^*, kcal/mol	2.98 [3.53]	1.65 [2.24]	5.47 [5.96]	4.05 [4.59]	5.88 [6.22]	4.64 [5.05]
λ_s,[d] kcal/mol	21.85	15.85	17.76	12.81	15.48	11.23
λ_v,[d] kcal/mol	15.95	15.95	23.34	23.34	25.27	25.27

[a] Difference in widths at half-height as a fraction of the total width at half-height, $(\Delta\nu_{hi} - \Delta\nu_{lo})/\Delta\nu_{1/2}$. The numbers quoted are certainly larger than is realistic for 4^+, where overlap with a higher energy band is serious on the high energy size of the CT band. [b] In kcal/mol. The number in brackets is the difference between λ and E_{op} using single-frequency vibronic coupling theory fits[15,16] to the CT bands (see text). [c] Unit, 10^3 cm^{-1}. Estimated using $\Delta\nu_{1/2}$ values obtained from band simulation using quartic diabatic surfaces. V_H is defined in eq 1, and $V_L = V_H(n_D)^{-1/2}$ [d] Estimated using eq 5.
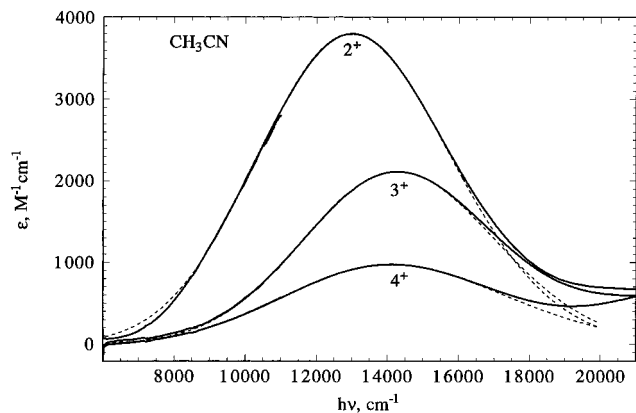

Figure 3. CT bands for 2^+–4^+ in acetonitrile with fits assuming adiabatic energy surfaces using eq 3 quartic-augmented diabatic energy surfaces superimposed as broken lines.

expected because it increases ϕ, by an average of 17.9° at the reduced hydrazine units and by 18.6° at the oxidized hydrazine units between 2^+ and 4^+. The V_H and V_L values estimated using the method described below are summarized in Table 6, where it will be seen that the V_L is less constant in AN and MC than V_H. The V_L values are almost the same as those obtained using a single frequency vibronic coupling analysis (not listed in Table 6).

The V values obtained for *p*-phenylenedihydrazine radical cations 2^+–4^+ reveal an important factor which causes these species to have charge localization, in contrast to *p*-phenylene-diamine 1^+, in which charge is delocalized. Assuming cos ϕ dependence of V, i.e. $V = V° \cos\phi_{neu} \cos\phi_{cat}$, with the ϕ values from the X-ray structures (see Table 2, averaging the three ϕ_{neu} values) produces $V_H° = 12.9$ kcal/mol for 4^+, and incrementing both ϕ_{neu} and ϕ_{cat} by the 6.2° difference between ϕ for 3^{2+} and 4^{2+} gives 13.6 kcal/mol for 3^+ and $V_H° = 12.6$ kcal/mol for 2^+. Although the ϕ values might be different in solution than in the solid, the dependence of V upon cos ϕ which is expected is at least approximately experimentally observed when the values obtained by X-ray are used. We consider the near constancy of the $V°$ values obtained to be a welcome check on the internal consistency of the V values appearing in Table 6.

$V°$ for *p*-phenylenedihydrazine cations are approximately one-half the 23.6 kcal/mol value estimated by Hush theory for the delocalized ($E_{op} = 2V$), untwisted 1^+.[1] A smaller $V°$ value with hydrazine charge-bearing units is expected because V depends on the interaction between the charge-bearing unit and the bridge,[17] and spin density at the aryl nitrogens is considerably smaller for hydrazine than for the amine charge-bearing units. In addition to larger λ, both the twist imposed by the bulky hydrazine substituents and the decrease in $V°$ are clearly important in causing 2^+–4^+ to be localized.

Discussion: Marcus–Hush Adiabatic Energy Surfaces

In Marcus–Hush theory, evaluation of λ for intervalence systems is trivial: $E_{op} = \lambda$ independent the other ET parameters. Sutin has published the analytical solutions for the ground and excited state adiabatic energy surfaces E_1 and E_2 obtained using the Marcus–Hush assumption that the diabatic energy surfaces are parabolas centered at 0 and 1 on the ET coordinate X ($H_{aa} = \lambda X^2$ and $H_{bb} = \lambda(1 - X)^2$).[10b] Interaction of these diabatic surfaces by the matrix element V produces eq 2 for the adiabatic

$$E_{1,2} = 0.5[\lambda(2X^2 - 2X + 1) + \Delta G°] \mp 0.5[\{\lambda(2X - 1) - \Delta G°\}^2 + 4V^2]^{1/2} \quad (2)$$

energy surfaces ($\Delta G° = 0$ for the symmetrical intervalence compounds discussed here). More recently, Creutz and co-workers have demonstrated eq 2 to apply for all values of V which give a double minimum surface ($V < \lambda/2$).[13] The maximum on the ground state E_1 surface occurs at $X_{max} = 0.5$, where $E_1 = E_{op}/4 - V$, and the minima at $X_{min} = (1/2)\{1 \pm (1 - [4V^2/\lambda^2])^{1/2}\}$, where $E_{1,min} = -V^2/\lambda$. As Hush pointed out, the $\Delta\nu_{1/2}$ produced by this energy surface is what he calls the "high-temperature limit" (htl) bandwidth, $\nu_{1/2}$(htl) = [(16 ln(2)$k_bT)E_{op}]^{1/2}$ = (2298.2E_{op})$^{1/2}$ at 25 °C. Hush also notes that observed intervalence complex CT bands are broader than $\nu_{1/2}$(htl). The CT bandwidth is expected to depend upon $h\nu_v$, and Hush used $g(h\nu,T) = [F \coth(F)]^{1/2}$, where $F = h\nu_v/2k_bT$ to describe the broadening,[11b] with $\nu_{1/2} = g(h\nu_v,T)\nu_{1/2}$(htl), while Winkler and co-workers break λ up into portions and only use

(17) Brouwer, A. M.; Wiering, P. G.; Zwier, J. M.; Langkilde, F. W.; Wilbrandt, R. *Acta Chem. Scand.* **1997**, *51*, 217.

a factor similar to $g(h\nu_v,T)$ for the higher frequencies employed.[18] In vibronic coupling theory the bandwidth depends upon the λ_s,λ_v partitioning as well as on $h\nu_v$.[14,15]

The simple $E_{op} = \lambda$ relationship no longer holds when vibronic coupling theory[14] is employed for consideration of ET reactions. Instead, the CT band position (E_{op}) and width at half-height ($\Delta\nu_{1/2}$) are influenced by all three of the ET parameters except V, i.e. λ_v, λ_s, and $h\nu_v$. Vibronic coupling theory allows simulation of CT absorption bands as a function of the ET parameters,[15] and we have recently discussed application of such calculations to σ-linked intervalence bis-hydrazines and bis-diazeniums.[16] We have more recently realized that vibronic coupling theory has unfortunately not been properly worked out either for absorption bands or rate constants in the strongly adiabatic regime, where V is large enough to make the electronic transmission coefficient effectively 1 and V does not appear in the preexponential term of the rate constant.[10] As previously discussed, use of averaged single-frequency $h\nu_v$ vibronic coupling theory for evaluation of the ET parameters produces rate constants which are significantly too small (k_{obs}/k_{calc} values ca. 20−50) for σ-linked bis-hydrazines, and this also occurs when such theory is applied to $\mathbf{3}^+$ and $\mathbf{4}^+$. Calculated rate constants are also too slow if adiabatic rate theory is used with eq 2 as the energy surfaces. We shall restrict our discussion here to trying to construct the proper adiabatic energy surfaces for $\mathbf{2}^+$−$\mathbf{4}^+$.

Discussion: Adiabatic Energy Surfaces using Quartic-Augmented Diabatic Energy Surfaces

We have not seen a discussion of the shape of diabatic energy surfaces E'_1 and E'_2 which will produce the broadened CT bands which are observed. It is necessary to obtain expressions for E'_1 and E'_2 if one is to simulate the CT band to more accurately obtain ET parameters which will allow proper calculation of the rate constant using adiabatic theory. Because use of parabolas for the diabatic energy surfaces leads to a band width of $\nu_{1/2}$(htl), the actual diabatic energy surfaces are not parabolas. The simplest expedient for obtaining energy surfaces which do produce the experimental band shape appears to us to be to introduce a quartic term in the diabatic energy surface. The use of fourth-order polynomials to generate empirical adiabatic energy surfaces,[19ab] including the construction of surfaces for two[19c] and multidimensional[19d] reaction coordinate cases applied to concerted reactions with more than one bond stretching at the transition state, and comparison with Marcus theory predictions has appeared, but we have not seen previous application of a quartic term in diabatic energy surfaces to allow construction of adiabatic energy surfaces. We use diabatic energy wells given by eq 3, including the $(1 + C)$ term in the

$$H'_{aa} = \{\lambda X^2/(1 + C)\}\{1 + C(X)^2\} \qquad (3a)$$

$$H'_{bb} = \{\lambda(X - 1)^2/(1 + C)\}\{1 + C(X - 1)^2\} \qquad (3b)$$

denominator to retain the $E_{op} = \lambda$ relation at $V = 0$. When $C = 0$, Hush's diabatic parabolas (H_{aa} and H_{bb}) are obtained, but when $C > 0$, the H'_{aa} and H'_{bb} energy wells are slightly broader than parabolas near the minima and rise more steeply and cross the parabolas at $X = 1$ and 0, respectively. Figure 4 shows a graphical comparison of the $C = 0$ parabolas with $C = 0.2$
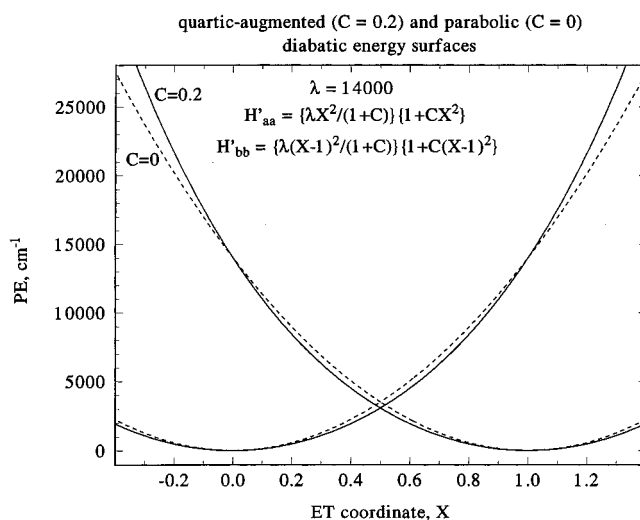
(18) Winkler, J. R.; Netzel, T. L.; Creutz, C.; Sutin, N. *J. Am. Chem. Soc.* **1987**, *109*, 2381.

(19) (a) Dunn, B. M. *Int. J. Chem. Kinet.* **1974**, *6*, 143. (b) le Noble, W. J.; Miller, A. R.; Harmann, S. D. *J. Org. Chem.* **1977**, *42*, 338. (c) Guthrie, J. P. *Can. J. Chem.* **1990**, *68*, 1643. (d) Guthrie, J. P. *J. Am. Chem. Soc.* **1996**, *118*, 12878, 12886.

Figure 4. Comparison of quartic-augmented diabatic energy surfaces using $C = 0.2$ with Hush's parabolic ($C = 0$) ones (shown for $\lambda = 14\,000$ cm^{-1}).
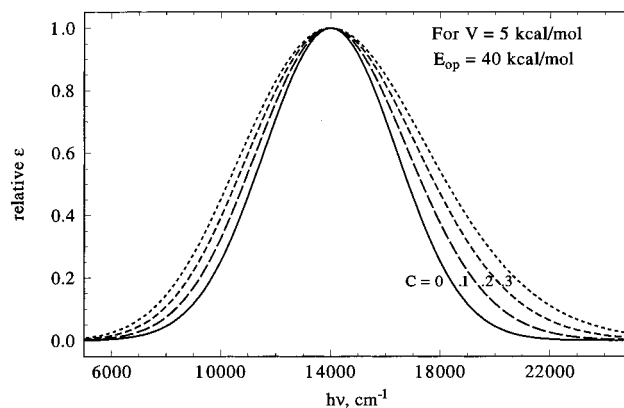

Figure 5. Calculated dependence of CT band shape upon C for quartic-augmented diabatic energy surfaces, shown for $V = 5$ kcal/mol (1750 cm^{-1}) and $\lambda = 40$ kcal/mol (14 000 cm^{-1}).

quartic-augmented curves. Like the parabolas, the quartic-augmented H'_{aa} and H'_{bb} curves cross at $X_{max} = 0.5$, but crossover occurs at $(\lambda/4)(1 + C/4)/(1 + C)$, increasingly smaller than $\lambda/4$ as C increases.

The CT band shape for the Classical theory of an adiabatic energy surface may be obtained using a simple Boltzmann weighting function, as we used earlier for averaging ESR spectra of hydrazine radical cations,[20] and showed not to require quantum mechanical corrections. For example, when $\epsilon_{rel} = \exp(-(E_1 - E_{1,min})/k_bT)$ is used with the eq 2 energy surface, the band width obtained is Hush's $\nu_{1/2}$(htl). Band widths on the order of those observed are obtained when C is on the order of 0.1−0.3 for λ values near the 14 000 cm^{-1} (40 kcal/mol) of the compounds under discussion. For a given λ, $\Delta\nu_{1/2}$ values rise as C is increased (see Figure 5). In contrast to the behavior for parabolic ($C = 0$) diabatic energy surfaces, where $E_{op} = \lambda$ and $\Delta\nu_{1/2}$ are independent of V, E_{op} becomes increasingly smaller than λ as V increases, more rapidly as C increases, and the band becomes increasingly unsymmetrical, with the high-$h\nu$ half-width larger than the low-$h\nu$ half-width, and depends weakly upon V. Both $E_{op} \neq \lambda$ and band asymmetry result from vibronic coupling theory calculations of band shape,[15,16] and band asymmetry in the direction calculated is experimentally observed (see Table 6). The C, λ, and V values obtained from simulation

(20) Nelsen, S. F.; Frigo, T. B.; Kim, Y. *J. Am. Chem. Soc.* **1989**, *111*, 5387.

of the CT bands using eq 3 for the diabatic energy surfaces are summarized in Table 6, and the band shape calculated using these parameters is compared with the experimental band shape in Figure 3. Band simulation is especially important for 4^+, where significant overlap with the tail of a higher energy band becomes clear. Although band shape is weakly dependent upon V, simulations giving indistinguishable fits to the experimental data using the same C values were obtained using V_H and V_L. The band shape simulations obtained using adiabatic theory are within experimental error of being the same as those using single-frequency vibronic coupling theory. The major differences in the parameters obtained using vibronic coupling theory and quartic-augmented diabatic curves with adiabatic theory are that the λ values obtained using adiabatic theory are significantly closer to E_{op} and that the λ_s, λ_v, $h\nu_v$ interactions which allow multiple fits to our data using vibronic coupling theory are not addressed. λ_s and λ_v prove not to be reasonably separated using vibronic coupling theory fits for intervalence bis-hydrazines anyway,[16] including the 2^+-4^+ studied here.

In contrast to using vibronic coupling theory, the ET rate constant calculated using adiabatic rate theory is rather insensitive to the separation of λ_v from λ_s, because this separation only affects the $(\lambda_v/\lambda)^{1/2}$ term in the preexponential factor. We estimate their separation here by employing the traditional Marcus dielectric continuum theory equation 4 for λ_s and assume

$$\lambda_s \text{ (kcal/mol)} = (332.1)\, g(r,d)\, \gamma,$$
$$\lambda_s \text{ (cm}^{-1}) = (1.162 \times 10^5)\, g(r,d)\, \gamma \quad (4a)$$

$$\gamma = (n_D{}^2)^{-1} - \epsilon_s{}^{-1} \quad\quad\quad (4b)$$

that λ_v is insensitive to solvent change.[10] The solvent polarity term γ is calculated from the static dielectric constant, ϵ_s, and the refractive index, n_D, and is 0.528 for AN and 0.383 for MC. The distance factor $g(r,d)$ of eq 4 was traditionally written $(r^{-1} - d^{-1})$ for intervalence complexes, where r is the radius of the charge-bearing unit and d is the ET distance as above. This is now not now believed to be a good assumption,[21,22] but $g(r,d)$ is not required to separate λ_s from λ_v if eq 4 holds and λ_v is the same in both solvents because $g(r,d)$ is then $(\lambda(\text{AN}) - \lambda(\text{MC}))/48.15$ using λ values in kilocalories/mole, which produces eq 5

$$\lambda_s(\text{AN}) \text{ (kcal/mol)} = 3.641[(\lambda(\text{AN}) - \lambda(\text{MC})],$$
$$\lambda_s(\text{AN}) \text{ (cm}^{-1}) = (1.273 \times 10^3)[(\lambda(\text{AN}) - \lambda(\text{MC})] \quad (5)$$

for $\lambda_s(\text{AN})$. λ_s and λ_v values using these assumptions are included in Table 6. Ion pairing in MC would invalidate eq 4 and 5, but we have found no evidence for ion pairing in MC either in intermolecular self-ET studies of bis-(N,N'-bicyclic)-hydrazines[23] or intramolecular ET studies of bis-(σ-bond-linked)-hydrazines,[16a,24] although ion pairing effects are clearly observed in the less polar solvent chloroform.[24] The λ_v values obtained using eq 5 appear to us to be reasonable. λ_v is estimated to

increase 9.4 kcal/mol as twisting is increased by the introduction of methyl groups in going from 2^+ to 4^+, but to remain significantly smaller for these aryl,*tert*-butyl-substituted diazabicyclooctanes than for alkyl,*tert*-butyl-substituted ones.[16a] The λ_s estimated decreases as methyl substitution increases, possibly because solvent cannot approach the aryl-substituted nitrogen as easily. The separation of λ_v and λ_s employed here may well not be correct[25] because, as indicated by the cyclic voltammetry data, there appears to be specific solvation of the oxidized hydrazine unit which is not accounted for by dielectric continuum theory. Getting λ_s and λ_v accurately separated is not very important for calculation of rate constants using adiabatic rate theory.

Discussion: Position of 2^+ on the ET Reaction Coordinate

The principal geometric changes characterizing oxidation of arylhydrazine units are decrease in $d(\text{NN})$, decrease in ψ-(CNNC), increase in $\phi(\text{lp},\pi)$, and decrease in $\alpha' = 120 - \alpha_{av}$ at the N-Ar nitrogen. These parameters are not independent of each other, but all change substantially. The similarity of the parameters for 5^+ with nitrate and tetraethynylborate counterions, which have very different shapes and sizes, suggests that crystal packing forces are not the principal determining factor for these geometric parameters. By all of these criteria, the difference between the two hydrazine units of 2^+ is smaller than that between our best available noninteracting models, 2^0 for the neutral units and 5^+ for the oxidized unit (we employ the average of the parameters for the two salts). To see whether the changes are significant, we list the difference in each parameter for 2^0 minus that for 5^+, the difference for the neutral and oxidized units of 2^+, and the difference in these changes (with the σ value for the measurements in parentheses): $\Delta d(\text{NN})$, 0.109 Å, 0.095 Å, difference 0.014 Å (σ 0.003 Å); $\Delta\psi(\text{CNNC})$, 50.3°, 40.0°, difference 10.3° (σ 0.3°); $\Delta\phi(\text{lp},\pi)$, $-18.6°$, $-15.0°$, 3.6° (σ 0.3°); $\Delta\alpha'$, 5.1°, 3.5°, difference 1.6° (σ 0.2°). Although the real uncertainty in the parameters is larger than σ and crystal packing forces will have some effect on these parameters, we conclude that the changes between the models and 2^+ are significant and that interaction between the hydrazine units of 2^+ can be directly observed in the structures determined. Quantitating the amount of interaction is difficult because the parameters are not expected to be linear with an electron transfer coordinate, but the fractional changes observed are 0.87 for $d(\text{NN})$, 0.80 for $\psi(\text{CNNC})$, 0.81 for $\psi(\text{lp},\pi)$, and 0.69 for α'. We do not have as good models for neutral units of 4^+, but the differences between the reduced and oxidized ends of 4^+ are larger than those for 2^+, and we believe that there is rather clearly significantly less interaction between the hydrazine units of this more twisted compound.

It is of interest to compare the above fractions for 2^+ with the fractional changes in position along the reaction coordinate, which is $1 - 2X_{min}$, because each minimum is shifted by X_{min} from the 0 and 1 resting points if V were 0 and there were no electronic interaction between the reduced and oxidized hydrazine units. The value obtained for X_{min} using the parameters of Table 6 (V_H has been employed) are solvent-dependent, principally because λ depends upon solvent. The values of (1

(21) (a) Brunschwig, B. S.; Ehrenson, S.; Sutin, N. *J. Phys. Chem.* **1986**, *90*, 3657. (b) Barbara, P. F; Meyer, T. J.; Ratner, M. A. *J. Phys. Chem.* **1996**, *100*, 13148.

(22) The traditional $(r^{-1} - d^{-1})$ expression for $g(r,d)$ is also inconsistent with our data. The values of r obtained using the 5.657 Å value of d employed in the evaluation of V for 4^+ are 12.0 and 10.3 Å, neither of which is physically reasonable. The average r for **5** estimated from the calculated molecular volume corresponds to a estimated r_{X-ray} of 4.32 Å, and the d values necessary to obtain such r values using the traditional expression are 3.08 and 3.22 Å, respectively.

(23) (a) Nelsen, S. F.; Kim, Y.; Blackstock, S. C. *J. Am. Chem. Soc.* **1988**, *111*, 2049. (b) Nelsen, S. F.; Wang, Y. *J. Org. Chem.* **1994**, *59*, 1655.

(24) (a) Nelsen, S. F.; Adamus, J.; Wolff, J. J. *J. Am. Chem. Soc.* **1994**, *116*, 1589. (b) Nelsen, S. F. *J. Am. Chem. Soc.* **1996**, *118*, 2047.

(25) We note that λ_s values obtained from solvent effects are not believed to be as significant as they once were because the low-frequency components of λ_v should be transferred to λ_s for the purposes of vibronic coupling theory. Hydrazines have especially large contributions of low-frequency components to λ_v, and as much as 1/3 of λ_v should be transferred to λ_s for saturated bis-N,N'-bicyclics.[24b]

(26) Nelsen, S. F.; Ismagilov, R. F.; Trieber, D. W. Submitted for publication.

$- 2X_{min}$) for 2^+ to 4^+ in AN are 0.91, 0.97, and 0.98, respectively, and in MC are 0.85, 0.95, and 0.97. These fractions approach 1.0 as aryl methyls are introduced and V decreases, as expected. It is not obvious what effective polarity a crystal should be assigned, but the ET parameters extracted from the CT band clearly predict that effects of electronic mixing should be seen for 2^+, and the fractions listed for d(NN), ψ(CNNC), and ψ(lp,π) bracket the $(1 - 2X_{min})$ value obtained for 4^+ in MC. We do not think such a result has been obtained previously and believe that it suggests that the adiabatic energy surface obtained by analysis of the CT bands is at least semiquantitatively correct.

Discussion: Comparison of Observed and Calculated Rate Constants

The adiabatic rate expression (eq 6)[10] is far less ambiguous to apply than vibronic coupling theory equations because the

$$k_{ad} = \nu_v(\lambda_v/\lambda)^{1/2} \exp(-\Delta G^*/RT) \qquad (6)$$

preexponential factor is only weakly dependent upon ν_v and upon the λ_v,λ_s separation, neither of which can be very well determined. Adiabatic rate theory appears to us to be basically an alternative to using vibronic coupling theory to estimate tunneling interactions. The E'_1 energy surface maximum calculated from the quartic-augmented diabatic energy surfaces of eq 3 is significantly lowered from the $\lambda/4 - V$ of Hush theory because the CT band broadening effects of $h\nu_v$ and λ_v are incorporated into the surface. The barrier obtained is rather broad and tunneling effects are assumed to be insignificant. ΔG^* in eq 6 is $E'_1(\text{max}) - E'_1(\text{min})$, which we have calculated numerically because an analytical expression for $E'_1(\text{min})$ has not been obtained. Values obtained from the CT band analyses are included at the end of Table 6.

Table 7 compares ratios of calculated adiabatic rate constants using room temperature ET parameter sets (Table 6) with k_{et} values extrapolated to 298 K (Table 5). The first column shows rate constants calculated using Hush theory ignoring tunneling. Agreement is good for 3^+ but the rate constant ratio is 1 order of magnitude smaller for 4^+. Hush always employed tunneling corrections. The second column shows the ratios obtained using Hush's tunneling expression, although it must be misapplied because it is only stated to be valid when $h\nu_v < 2RT$ and $h\nu_v = 800$ cm^{-1} is 1.9($2RT$) at room temperature. Including tunneling makes the calculated rate constants too large. Hush theory does not fit the observed CT bands (Figure 5, $C = 0$ corresponds to Hush theory; Table 6 shows the observed C values). The third column of Table 7 shows the ratios obtained using ET parameters derived from quartic-augmented diabatic surfaces, which do fit the observed bands. The calculations are within experimental error for all four data sets, when it is considered that extrapolations of the ESR data averaging 50° for AN and 100° for MC are necessary to get to room temperature, where the CT band analysis was done. We shall discuss applying quartic-augmented energy surfaces to other systems elsewhere.[26]

Conclusions

Hydrazines linked by a *p*-phenylene bridging unit are charge-localized in the intervalence oxidation state, and properly choosing substituents allows the isolation of compounds in 0, 1+, and 2+ oxidation states which are stable enough for a variety of physical studies. The use of triplet state dipolar splitting constants to estimate d_{esr} of the dication bis-radicals appears to allow a reasonable estimation of how much the

Table 7. Ratio of Calculated k_{ad} to ESR-Determined k_{et} for 3^+ and $4^{+\ a}$

	Hush Theory[b] ignoring tunneling	Hush Theory[b] with tunneling[c]	quartic-augmented, no tunneling[d]
3^+ (AN)	1.6	20	1.6
3^+ (MC)	2.9	34	3.5
4^+ (AN)	0.15	2.2	0.6
4^+ (MC)	0.21	3.0	1.1

[a] Calculated at 298 K with $h\nu_v = 800$ cm^{-1}. [b] Using V_H with $\lambda = E_{op}$ (parabolic energy surfaces). λ_s and λ_v were scaled by E_{op}/λ from the values used for the quartic-augmented surfaces. [c] Using Hush's tunneling factor,[11b] eq 7, where $F = h\nu_v/4RT$. This tunneling factor is only supposed to be applicable when $h\nu_v < 2RT$. [d] Parameters of Table 6 with V_L.

$$\Gamma = [2F \operatorname{csch}(2F)]^{-1/2} \exp\{-(\lambda_v/h\nu_v)(\tanh[F] - F)\} \qquad (7)$$

effective distance between the charge bearing centers is affected by delocalization into the bridge, which we used to obtain better d values to use in estimating V for the radical cations. The compounds studied have V_H in the range 7.2−3.1 kcal/mol, placing their intramolecular ET processes in the adiabatic range. The use of quartic-augmented diabatic curves in obtaining adiabatic energy surfaces allows fitting the calculated CT bands to experiment and, for 4^+, which gives the best ESR rate data for technical reasons, gives calculated rate constants which are surprisingly close to the experimental data. Tunneling "corrections" are rather clearly not necessary when the adiabatic lower surface, which is revealed experimentally by the IV-CT band, is employed. The present analysis also predicts that the geometry of the oxidized and reduced units of 2^+ should be detectably different from those for localized models, which is observed experimentally, and the V values obtained are consistent with the N-lone pair, π-aryl twist values determined by X-ray crystallography. We are currently studying other π-bridged cations which vary the distance and twist angles between the charge bearing units and the bridge, and also vary the bridge orbital energies, to better understand the factors controlling ET rates in π-linked compounds.

Experimental Section

UV/vis spectra were obtained on a Hewlett-Packard HP 8452 diode array spectrophotometer (190−820 nm range) or Perkin Elmer Lambda 20 UV/vis spectrometer (190−1100 nm). A Nicolet 740 IR spectrometer was used to obtain NIR spectra. NMR spectra were acquired on Bruker AM-500 or AC-300 instruments. ESR spectra were obtained on a Bruker ESR 300E spectrometer. Preparations and crystallographic data for **2**, **2$^+$Ph$_4$B$^-$**, and **5$^+$NO$_3$** appear in the Supporting Information for ref 1.

1,4-Bis(2-*tert*-butyl-2,3-diazabicyclo[2.2.2]oct-3-yl)-2,5-dimethyl-benzene-1,4-diyl (3). 1,4-Diiodo-2,5-dimethylbenzene (179 mg, 0.50 mmol) was placed into an oven-dried 50 mL Schlenk flask under nitrogen. THF (3 mL) was added, and the mixture was cooled to −78 °C. *t*-BuLi (1.74 M in pentane, 1.15 mL, 2.00 mmol) was added slowly. The mixture was stirred for 40 min to give a white suspension and a yellow precipitate of 1,4-dilithio-2,5-dimethylbenzene to which yellow 2-*tert*-butyl-2,3-diazabicyclo[2.2.2]oct-2-ene iodide (294 mg, 1.00 mmol) was added. The mixture was stirred for 20 min, and the cooling bath was gradually lowered. After the yellow color disappeared (ca. 2 h), the mixture was stirred for additional 30 min and quenched with water (15 mL), extracted with toluene (3 × 20 mL), dried with MgSO$_4$, and evaporated to give 0.22 g of white-yellow solid. It was dissolved in refluxing toluene (3 mL) and cooled to 50 °C. CH$_3$CN (30 mL) was added in small portions over 2 h. Colorless crystals of pure 3 formed (182 mg, 83%), mp 263−264 °C. MS: *m/e* 438.3732, *I* = 21.7%, calcd for C$_{28}$H$_{46}$N$_4$ 438.3722. ^{1}H NMR (500 MHz, C$_6$D$_6$): δ 7.91 and 7.85 (s., 2H, Ar*H*), 3.21 (br. s., 2H, NC*H*), 2.98 and 2.92 (br. s., 2H, NC*H*), 2.38 and 2.37 (s., 6H, C*H*$_3$), 2.23 (m., 2H, C*H*$_2$), 2.19 (m., 2H, C*H*$_2$), 1.83 (m., 4H, C*H*$_2$), 1.49 (m., 4H, C*H*$_2$), 1.14 (m., 2H,

CH_2), 1.11 (s., 18H, C(CH_3)$_3$), 0.99 (m., 2H, CH_2). ^{13}C{^{1}H} NMR (125 MHz, C$_6$D$_6$): δ 148.40 and 148.15 (NC_{ar}), 126.93 and 126.47 (C_{ar}CH$_3$), 125.52 and 125.10 (C_{ar}H), 58.90 and 58.75 (C(CH$_3$)$_3$), 51.52 and 51.33 (NCH), 46.506 (NCH), 30.03 and 29.95 (CH$_2$), 29.05 and 28.99 (C(CH$_3$)$_3$), 27.01 (CH$_2$), 23.37 and 23.32 (CH$_2$), 20.76 and 20.44 (CH$_2$), 18.67 and 18.46 (CH$_3$).

1,4-Bis(2-*tert*-butyl-2,3-diazabicyclo[2.2.2]oct-3-yl)-2,3,5,6-tetra-methylbenzene-1,4-diyl (4). 1,4-Diiodo-2,3,5,6-dimethylbenzene (211 mg, 0.55 mmol) was placed into an oven-dried 50 mL Schlenk flask under N$_2$. THF (3 mL) was added, and the mixture was cooled to −78 °C. *t*-BuLi (1.6 M in pentane, 1.20 mL, 1.92 mmol) was added slowly. The mixture was stirred for 30 min to give a pale yellow suspension, and then 2-*tert*-butyl-2,3-diazabicyclo[2.2.2]oct-2-ene iodide (300 mg, 1.02 mmol) was added. The mixture was stirred for 5 min, and the cooling bath was gradually lowered and then removed. After the yellow color disappeared (*ca.* 45 min), the mixture was stirred for additional 10 min and then quenched with water (15 mL), extracted with toluene (3 × 30 mL), and evaporated to give 0.29 g of off-white solid. The solid was dissolved in toluene (5 mL), and CH$_3$CN (*ca.* 5 mL) was added to precipitate out a white solid (132 mg, 51%). The solution was cooled to obtain more product (40 mg, 16%), mp 248−249 °C. MS: *m/e* 466.4025, *I* = 65%, calcd for C$_{30}$H$_{50}$N$_4$ 466.4035. ^{1}H NMR (500 MHz, C$_6$D$_6$): δ 3.18 (br. s., 2H, NCH), 3.08 and 3.04 and 3.02 and 3.00 (s., 6H, CH_3), 2.79 and 2.73 (br. s., 2H, NCH), 2.55 (m., 2H, CH_2), 2.53 and 2.52 and 2.51 and 2.49 (s., 6H, CH_3), 2.32 (m., 2H, CH_2), 1.90 (m., 2H, CH_2), 1.48 (tq., *J* = 12.7, 3.0 Hz, 2H, CH_2), 1.41 (m., 2H, CH_2), 1.20−1.27 (m., 6H, CH_2), 1.11 and 1.10 (s., 18H, C(CH_3)$_3$). ^{13}C NMR {^{1}H} (125 MHz, C$_6$D$_6$): δ 146.18 and 145.77 and 145.65 and 145.37 (NC_{ar}), 132.08 and 131.89 and 131.61 and 131.28 and 131.25 and 130.91 and 130.72 and 130.52 (C_{ar}CH$_3$), 59.92 and 59.60 and 59.56 (C(CH$_3$)$_3$), 54.91 and 54.74 and 54.69 and 54.67 (NCH), 47.39 and 47.34 and 47.29 and 47.24 (NCH), 29.23 and 29.03 and 28.97 (CH$_2$), 29.13 (C(CH$_3$)$_3$), 27.20 and 27.14 and 27.06 (CH$_2$), 24.49 and 24.40 (CH$_2$), 22.62 and 22.58 and 22.22 (CH$_2$), 17.69, 17.40, 17.27, 17.06, 16.87, 16.83, 16.52, and 16.44 (C_{ar}CH$_3$).

Crystallization of 1,4-Bis(2-*tert*-butyl-2,3-diazabicyclo[2.2.2]oct-3-yl)-2,3,5,6-tetramethylbenzene-1,4-diyl Radical Cation Tetraphen-ylborate (4$^+$BPh$_4$$^-$). To a solution of **4** (7.5 mg, 0.016 mmol) in CH$_2$Cl$_2$ (3 mL) was added AgNO$_3$ (0.0229 M in CH$_3$CN, 700 μL, 0.016 mmol), and the mixture was stirred for 15 min and centrifuged. NaBPh$_4$ (6.3 mg, 0.018 mmol) was added, and the mixture was evaporated to give a green solid. Addition of chloroform resulted in a green solution and a white precipitate (NaNO$_3$) that was filtered off. The solution was evaporated and dissolved in wet CH$_3$CN (1.5 mL) in a small test tube that was placed into a jar with water overnight. Dark green blocks with metallic luster formed in the test tube. Identity of the product was proven by X-ray crystallography.

1,4-Bis(2-*tert*-butyl-2,3-diazabicyclo[2.2.2]oct-3-yl)-2,3,5,6-tetra-methylbenzene-1,4-diyl Bis(radical cation hexafluoroantimonate) (4^{2+}(SbF$_6$$^-$)$_2$). AgSbF$_6$ (76.1 mg, 0.221 mmol) was weighed out in a 50 mL Schlenk flask under nitrogen, dissolved in CH$_2$Cl$_2$ (10 mL),

and cooled to −78 °C. 1,4-Bis(2-*tert*-butyl-2,3-diazabicyclo[2.2.2]oct-3-yl)-2,3,5,6-tetramethylbenzene-1,4-diyl (**4**) (51.6 mg, 0.111 mmol) was added, the mixture was stirred for 3 min, and the cooling bath was removed. The mixture was stirred for 3 h and then filtered through Celite. Some of the product stayed on the filter and was washed down with acetonitrile to give a dark-brown solution. Evaporation of the solution followed by recrystallization by vapor diffusion of ether into acetonitrile afforded 88 mg (85%) of the product. UV/vis in acetoni-trile: 446 nm (ε = 2.1 × 10^3), 338 nm (ε = 5.6 × 10^3), 280 nm (ε = 6.3 × 10^3), and 256 nm (ε = 4.2 × 10^3). The two latter absorption bands overlap with a very strong (ε > 20 × 10^3) band at 208 nm, and the ε values are slightly concentration-dependent.

NMR of Bis-hydrazine Radical Cations. In a typical experiment, 1,4-bis(2-*tert*-butyl-2,3-diazabicyclo[2.2.2]oct-3-yl)-2,3,5,6-tetrameth-ylbenzene-1,4-diyl (**4**) (30.0 mg, 0.0643 mmol) was placed under nitrogen in a small test tube with AgNO$_3$ (12.0 mg, 0.0706 mmol). CD$_2$Cl$_2$ (400 μL) was added, and the mixture was stirred vigorously for 3 h and then centrifuged. The solution was carefully decanted with a microliter syringe through the septum, then the test tube was rinsed with some more CD$_2$Cl$_2$ to the final volume of 550 μL. A spectrum was collected and then DBNO was added in 20 μL and then 40 μL aliquots. Neat DBNO was assumed to be 5.96 M, and the total radical concentrations were calculated accordingly. The NMR experiment for 1,4-bis(2-*tert*-butyl-2,3-diazabicyclo[2.2.2]oct-3-yl)benzene-1,4-diyl radi-cal cation (**2$^+$**) was conducted at −16.3 °C.

Preparation of Radical Cation Solutions for Optical and ESR Studies. In a typical experiment, AgNO$_3$ (1.85 mg, 1.09 mmol) and **4** (5.10 mg, 0.0109 mmol) were placed in a dry Pyrex test tube under nitrogen. CH$_2$Cl$_2$ (2.5 mL) was added and the mixture was vigorously stirred under nitrogen for 7 h. The test tube was centrifuged, and the green solution was transferred to a 10 mL volumetric flask and diluted to the mark with CH$_2$Cl$_2$. The resulting solution was used for ESR measurements after brief degassing with N$_2$. Dilution to various concentrations provided solutions for the optical studies. Oxidations in CH$_3$CN were done with a freshly prepared stock solution of AgNO$_3$. Oxidations of **3** were conducted at 0−5 °C and those of **2** at −5 to 0 °C.

Supporting Information Available: Crystallographic data for **5$^+$**(B(C$_2$H)$_4$$^-$, **3^{2+}**BPh$_4$$^-$, **4$^+$**BPh$_4$$^-$, and **4^{2+}**(BPh$_4$$^-$)$_2$, num-bered thermal ellipsoid drawings, and heavy atom positions (15 pages). See any current masthead page for ordering and Internet access information.

JA9720321